First-Principles Studies in Mg-based Hydrogen Storage Materials：A Review

XiuBo Xie[a]*, Chuanxin Hou[a], Chunguang Chen[c], Xueqin Sun[a], Yu Pang[d], Yuping Zhang[a], Ronghai Yu[b]*, Bing Wang[e], Wei Du[a]*

[a]School of Environmental and Material Engineering, Yantai University, No. 30 Qingquan Road, Shandong, 264005, China

[b]Key Laboratory of Aerospace Materials and Performance (Ministry of Education) School of Materials Science and Engineering, Beihang University, No.37 Xueyuan Road, Beijing 100191, China.

[c]IEK 9, Forschungszentrum Jülich, D-52425 Jülich, Germany.

[d]Goodix Technology, 610041, Chengdu, China.

[e]Key Laboratory for Biomedical Effects of Nanomaterials and Nanosafety, Institute of High Energy Physics, Chinese Academy of Sciences, Beijing 100049, China.

*Corresponding author: Email address: xiuboxie@ytu.edu.cn; rhyu@buaa.edu.cn; duwei@ytu.edu.cn

Abstract

Hydrogen storage efficiency is essential for a booming clean hydrogen energy economy. Mg-based hydrogen storage materials have been intensively investigated due to their advantages of high theoretical storage capacity, satisfactory reversibility and natural abundance. However, the high thermal stability of Mg-H bonds leads to a high dehydrogenation temperature and sluggish kinetics. The construction of models for examining the interactions of hydrogen with Mg(MgH_2) and the catalytic

mechanism of catalyst additives is important. Therefore, this paper reviews recent advances in modelling and focuses on first-principles calculation applications in hydrogen adsorption, dissociation and diffusion energy calculations on Mg(0001) and high indexed Mg($10\bar{1}3$) surfaces with element doping, strain and alloy additives. The applications of first-principles calculations on the particle size and dehydrogenation of MgH_2 are also reviewed.

Keywords: First principles, magnesium, hydrogen energy storage

1. Introduction

Hydrogen energy possesses the advantages of being highly accessible, clean and of high calorific value. With the setting of deadlines for discontinuing the use of conventional fuel vehicles in countries all over the world, the utilization of hydrogen energy would be a promising development strategy for these countries. The construction of effective hydrogen storage materials is essential for realizing this objective [1-3]. Mg-based hydrogen storage materials are regarded as one of the most promising hydrogen storage media due to their multiple advantages [4-8]. Mg is an abundant element on earth with a high theoretical hydrogen storage capacity of 7.6 wt% [9], and its high reversibility [10], cycle stability and poison-resistance [11,12] render it promising for energy conversion, fuel cells and heat storage applications in the future. Mg exhibits a hexagonal crystal structure and changes into tetragonal and/or orthorhombic structures in the hydrogenated state [13]. MgH_2, in both the β and γ unit cell structures, can store hydrogen, and the γ phase tends to change into β-MgH_2 above 623 K [14-16]. Unfortunately, the disadvantages of high operating

temperature and sluggish (de-)hydrogenation kinetics hinder its large-scale application in expanding the hydrogen economy [17,18].

Intensive studies have been conducted on improving the kinetics and the thermodynamic performance of Mg-based hydrogen storage materials. The use of additives with positive catalytic activation, which include lightweight elements [19], transition metals [10,20] and their oxides [11,12,21-23], carbides [24-26], halides [27-29] and other compounds [30-33], has been widely investigated in recent years. Decorated particles and shell-like additives on the surface can prevent Mg particles from oxidizing and aggregating during hydrogenation and dehydrogenation cycles [31,34-37]. These additives can enhance the hydrogen storage kinetics of Mg by decreasing the activation energies [35,37]. Many experimental studies have been conducted to explain the catalytic effects of catalyst addition and nanosizing [38-41]. However, an intuitive understanding at the atomic scale is difficult to realize, except via calculations. With the development of computational materials science, the enthalpy for dehydrogenation of MgH_2 in several nanometers is calculated to be significantly reduced [42-45], indicating that the Mg-H band should be weakened with decreasing particle size. These calculation results have been supported by experiments in Mg and Mg-C systems [46-48]. In addition, the hydrogen diffusion distance can be undoubtedly decreased, which may facilitate the enhancement of the kinetic performance. Given the general recognition that cluster calculations show positive effects on the thermodynamic performance, recent studies have focused mainly on obtaining nanometre particles experimentally rather than via calculations.

Another important application of computational materials science is the simulation of the influences of catalysts on the structural stability and the orbital interactions between Mg and hydrogen atoms, which is beneficial for better understanding the hydrogen storage mechanism in various stages.

The hydrogen storage cycle contains hydrogen molecule adsorption, dissociation, hydrogen atom adsorption on the Mg surface, diffusion of H atoms into the Mg core, formation of MgH_2 and hydrogen release from MgH_2. Moreover, the particle size shows important influences on the hydrogen desorption energies. To clarify the interaction of hydrogen with the Mg and MgH_2 surfaces, we summarized the recent advances of first principles calculation applications for the hydrogen storage of Mg in different stages and the particle size effects on the desorption energy. The calculation details are introduced in Section 2. The related calculation results are summarized in Section 3, and suggestions are presented in Section 4.

2. Calculation Methods

The Vienna *ab initio* simulation package (VASP) is a complex package tool for conducting *ab initio* quantum-mechanical molecular dynamics simulations using pseudopotentials or the projector-augmented wave method and a plane wave basis set [49,50]. For Mg-based materials, the projector augmented wave (PAW) method is typically applied to examine the electron-ionic interaction [51-53]. The Perdew-Burke-Ernzerhof (PBE) with generalized gradient approximation (GGA) scheme is used for the exchange and correlation functional [54]. The plane wave expansion cutoff energies and integration over the Brillouin zone [55] under the

Monkhorst-Pack scheme for various systems should be tested prior to calculations based on the constructed models. The converged force on each atom for the internal optimization and a vacuum should be set in the calculation process. The climbing image nudged elastic band (NEB) [56,57] is applied to identify the minimum energy path (MEP) and the corresponding diffusion barrier, dissociation energy barrier for the slab models. Materials Studio can also be exploited for material calculations, and the Cambridge sequential total energy package [58,59] and Dmol3 codes [60,61] can also be applied to calculate the energy barriers for hydrogen absorption, dissociation and diffusion processes. Herein, we do not describe the calculation factor selections in detail due to the familiar settings with VASP calculations.

3. Applications of first principles calculation in the hydrogen storage of Mg-based materials

3.1 Hydrogen adsorption on Mg surfaces

3.1.1 Hydrogen adsorption on pure Mg and element doping surfaces

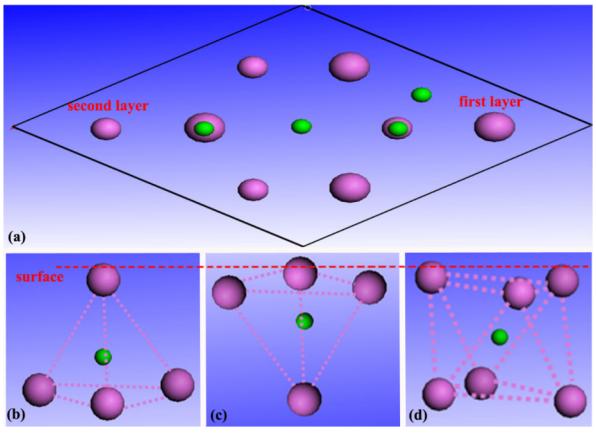

Figure 1. *Different hydrogen adsorption sites on Mg slab: (a) surface, (b) top tetrahedral interstices, (c) blow tetrahedral interstices and (d) octahedral interstice at the second layer [62]. Reproduced with permission from [62],copyright 2020*

The hydrogen atom adsorption on Mg(0001) slabs is calculated mostly for the pure Mg system. Generally, there are four different adsorption sites of Mg-Mg bridges, Mg top, fcc-hollow and hcp-hollow on the surface and three adsorption sites, namely, tetrahedral-1, tetrahedral-2 and octahedral on the subsurface, see Fig. 1 [49,62]. The adsorption energy is mainly calculated in the literature via the following equation: $E_{\text{ads}}^{H} = \frac{1}{N}(E_{Mg(0001)/H} - E_{Mg(0001)} - \frac{N}{2} \times E_{H_2})$ [49], where E_{ads} is the absorption energy of hydrogen, $E_{Mg(0001)/H}$ is the total energy of the H-adsorbed Mg(0001) slab, $E_{Mg(0001)}$ is the total energy of the pure Mg slab, E_{H_2} is the total energy of H_2 and N is the number of hydrogen molecules that are adsorbed in the system. Studies show that the fcc-hollow site and the tetrahedral site are the energetically favourable sites for hydrogen adsorption [63,64]. The adsorption energies for Mg(0001) surfaces that were doped with transition metal atoms, such as V, Nb, Ti, Fe, and Zr, were systematically calculated in recent years [65-69], which indicated that the impurities can decrease the energies. Tang *et al.* found that biaxial strain effectively enhances the hydrogenation performance of the H-Mg-H trilayer precursor due to the smaller lattice constant than that of Mg, and the precursor can be modulated by compressive and tensile stains during the hydrogenation process [70]. The H atoms gradually left Zr atoms for Mg atoms with the size growth of the Mg_nZr clusters, and the chemisorption energy of hydrogen for Mg_4ZrH_2 was the lowest among the cluster samples [71].

3.1.2 Hydrogen adsorption on Mg-metal or alloy interfaces

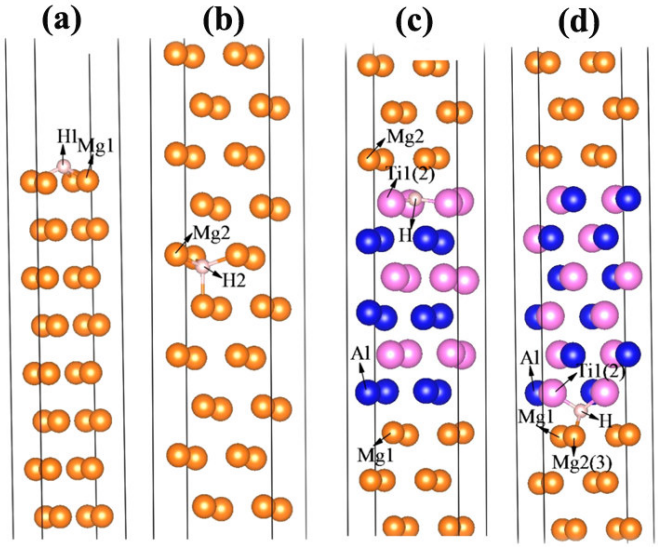

Figure 2. *Hydrogen adsorption sites at (a) surface and (b) inner of Mg(0001) slab, (c) Mg(0001)/TiAl(111) interface, (d) Mg(0001)/TiAl(110) interface [74]. Reproduced with permission from [74], copyright 2013 American Chemical Society.*

The construction of Mg/catalyst interfaces is important for investigating the hydrogen storage properties. Song *et al.* calculated the stability and hydrogen adsorption on the interfaces of Mg/Ti [72], Mg/Mg_2Ni [73], Mg/TiAl [74] and Mg/$TiMn_2$ [75] slabs. The anti-symmetrical configuration was found to be the most stable, and the hydrogen in the Ti environment was more concentrated than in the Mg environment, which means that Ti can act as a hydrogen atom captor. In the Mg/Mg_2Ni interface system, the Mg-Ni interaction across the interface was the main factor for stabilizing the interface, and the adsorbed hydrogen atoms in the interface may form covalent bonds with metal atoms. The strength of the H-metal bonds depended on the environment in which the H was located [73]. For the Mg/TiAl

system, Song and co-workers found that the formation energies of both the Mg(0001)/TiAl(110) and Mg(0001)/TiAl(111) interfaces were less than that of the Mg(0001) slab. The hydrogen adsorption energies at Ti-bri for Mg(0001)/TiAl(110), of -1.241 eV, and at Al-fcc for Mg(0001)/TiAl(111) of -0.333 eV were lower than the adsorption energy for the pure Mg(0001) surface of 0.089 eV. The experimental results also supported the satisfactory catalytic effects of the TiAl alloy [76]. Studies suggested that the total energy of the Mg/$TiMn_2$-Mn interface was smaller than that of the Mg/$TiMn_2$-Ti interface; hence, the interaction between Mg and Mn was stronger than that between Mg and Ti. According to additional calculation results, the hcp site near the Mn atom was the most stable site for hydrogen adsorbed on Mg/$TiMn_2$ interface. Bhatnagar *et al.* found that the location of TiH_2 beneath the Mg(0001) surface was energetically preferred over location on top of Mg [77].

3.2 Hydrogen dissociation energies

The hydrogen dissociation energy is very high on the pure Mg surface [78]. To modify the surface performance, Han *et al.* reported that the vacancy defect on the Mg(0001) surface was advantageous for the hydrogen dissociation process with an energy barrier of 1.28 eV, which was smaller than that of the defect-free surface of 1.42 eV [79]. The dissociation barrier was linearly reduced in the tensile strain region when the strain changed from compressive to tensile [80]. The dissociation energy was almost unchanged in the high-indexed Mg $(10\bar{1}3)$ surface compared to the Mg(0001) surface [81]. Calculations also suggested that the transition metals on the left of the periodic table preferred to substitute Mg in the second layer and others in

the first layer. For instance, the Fe on the right table displayed great impact on the dissociation barriers of hydrogen, while the element on the left showed little influence on the dissociation barriers [64].. Correspondingly, the transition metals that were doped on the Mg(0001) surface, such as Ni, V and Nb, tended to substitute the Mg atom in the second layer and catalyzed the dissolution of hydrogen [82,83]. The hydrogen initially moved to the surface and dissociated into two hollow sites before one H moved to the next hollow site. Then, the diffusion barriers of hydrogen atoms from the adsorption site to the next hollow site were significantly reduced with Ni, V and Nb dopings, and thu, the dehydrogenation process was improved. However, the co-doped system showed that Ni and V preferred to substitute Mg atoms from the first and second layers, respectively, and the Ni on the surface more significantly reduced the dissociation barrier of the hydrogen molecule compared to single dopings. The atomic Ni better facilitated H_2 dissociation than the ball-milled Mg that was incorporated with nano-Ni [84]. To further examine the catalytic performance of the AlV_3 nanocatalyst on the core@shell $Mg@Mg_{17}Al_{12}$ nanocomposite in Fig. 3a, Xie *et al.* investigated [62] the hydrogen dissociation of hydrogen molecules on the AlV_3 (001) surface. The site preferences of hydrogen atoms on the AlV_3 surface were considered, and hydrogen molecules adsorbed on the Al-Al bridge with a vertical attitude was calculated to be the most stable (see Fig. 3b-d), which differs from the molecular rotation attitude of 21° on the pure Mg(0001) surface [85]. The attitude of the hydrogen molecule during the dissociation process changed to parallel, and the dissociation energy was 0.76 eV (see Fig. 3e), which is much lower than that of Mg

(0.92 eV) with the same calculation conditions, indicating that AlV_3 exhibited satisfactory catalytic activation.

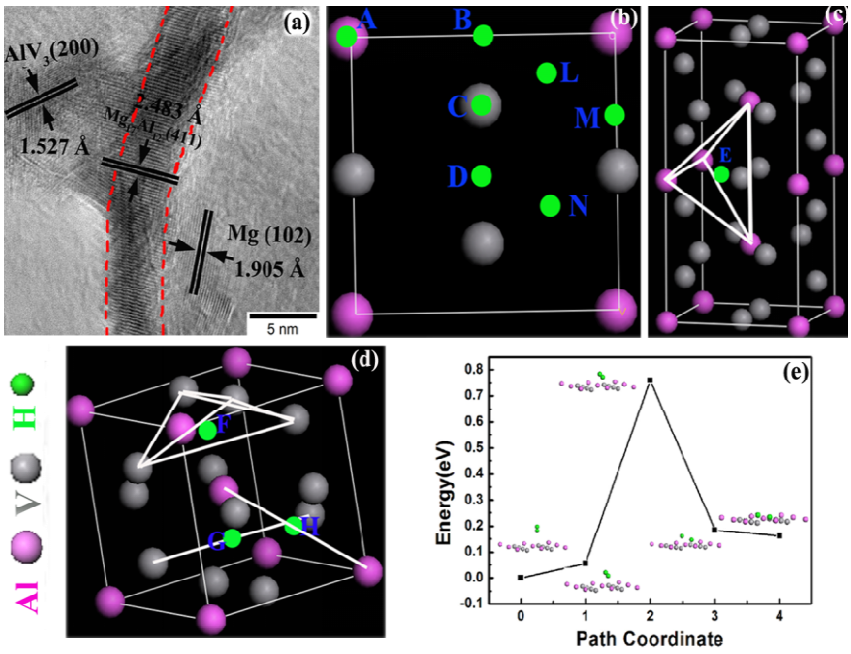

Figure 3 *(a) TEM image of AlV_3 decorated $Mg@Mg_{17}Al_{12}$ nanocomposite, (b-d) calculated absorption sites for hydrogen at AlV_3 surface and (e) dissociation barrier diagrams of hydrogen molecules on AlV_3 surfaces [62]. Reproduced with permission from [62], copyright 2020 American Chemical Society.*

3.3 Hydrogen diffusion in doped Mg surfaces and Mg/catalyst interfaces

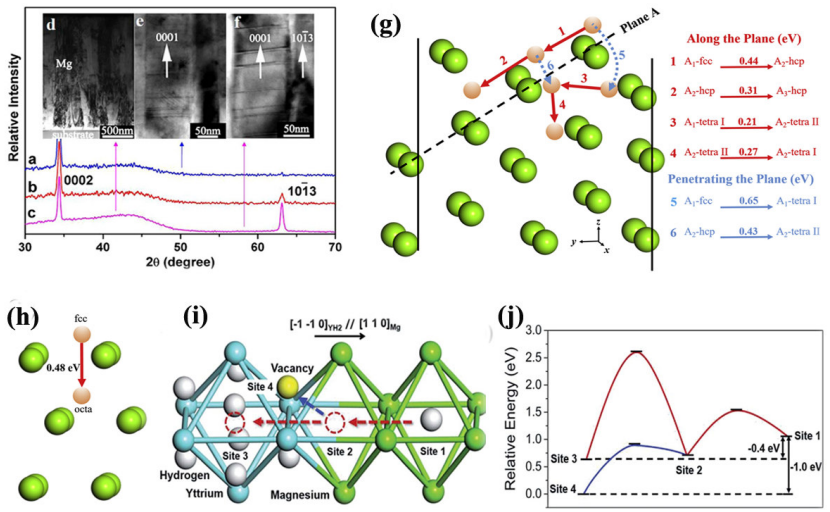

Figure 4. *X-ray diffraction (XRD) patterns of Mg thin film deposited at (a) 1.4×10^{-2} Pa, (b) 5.6×10^{-1} Pa and (c) 1.4×10^{-1} Pa, respectively. XTEM images of the (d) Mg thin film, films with (e) Mg (0001) texture and (f) (0001)+$(10\bar{1}3)$ texture. The pathways and energy barriers of H penetration on (g) Mg$(10\bar{1}3)$ and (h) Mg(0001) surfaces [81,87]. Reproduced with permissions from [81], copyright 2019 Elsevier and [87] 2015 Nature Publishing. Migration paths (i) and corresponding energy barriers (j) for hydrogen atoms at the Mg/YH_2 interface [89]. Reproduced with permission from [89], copyright 2017 Royal Society of Chemistry.*

On the Mg(0001) surface, Sun *et al.* found that there were two equal diffusion pathways for hydrogen atoms on the surface with a barrier of 0.45 eV. Another barrier of 0.31 eV was needed for further diffusion of hydrogen into the bulk region [65]. The incorporated Ni atom on the Mg surface easily dissociated hydrogen molecules and rendered H diffusion a rate-limiting step for hydrogenation [84]. Moreover, the substitution of Nb and Ti in the inner layers rather than in the outermost layer can facilitate the diffusion of hydrogen atoms via the formation of an H-Mg-H trilayer. Al and In were less useful for this process [86]. The vacancies that were induced by doping promoted the hydrogen diffusion process with diffusion paths of spiral channels formed by staggered octahedral and tetrahedral interstitials [79]. Lin *et al.* studied the hydrogen storage performance of Mg films with coexisting (0001) and $(10\bar{1}3)$ preferential orientations and found that the adsorption temperature was significantly decreased from 573 K to 392 K (see Fig. 4a-4f). According to additional

calculations, the diffusion energy barrier for the Mg($10\bar{1}3$) slab was much lower than that for the Mg(0001) slab (see Fig. 4 g-4 h), while the minimum energy path barriers for the Mg ($10\bar{1}3$) and Mg (0001) slabs were comparable, indicating the decrease in the experimental operating temperature was caused mainly by the diffusion advantages of the high-index surface rather than the dissociation process [81,87,88]. Another calculation study showed that the high affinity between Y and H promoted a decrease in the diffusion energy barrier, and the transition energy from site 2 to site 4 in Fig. 4i and 4j of the interface was only 0.2 eV [89]. In the NbH_2-Mg-Mg_2Ni composite, H atoms were transferred from the 4b site of NdH_{3-x} to the octahedral interstitial sites of the interface along the Mg [$1\bar{1}00$] direction [90]. Kumar *et al.* calculated the hydrogen diffusion pathways and barriers for Pd/Mg, Pd/MgO and Pb/MgH_2 (see Fig. 5). The formation of the MgO layer substantially increased the energy barriers for hydrogen diffusion, whereas hydrogenation became increasingly difficult through already established hydride domains. The Pd underwent a strain-induced crystallographic phase transformation near the interface, and the hydride domains suppressed hydrogen diffusion [91].

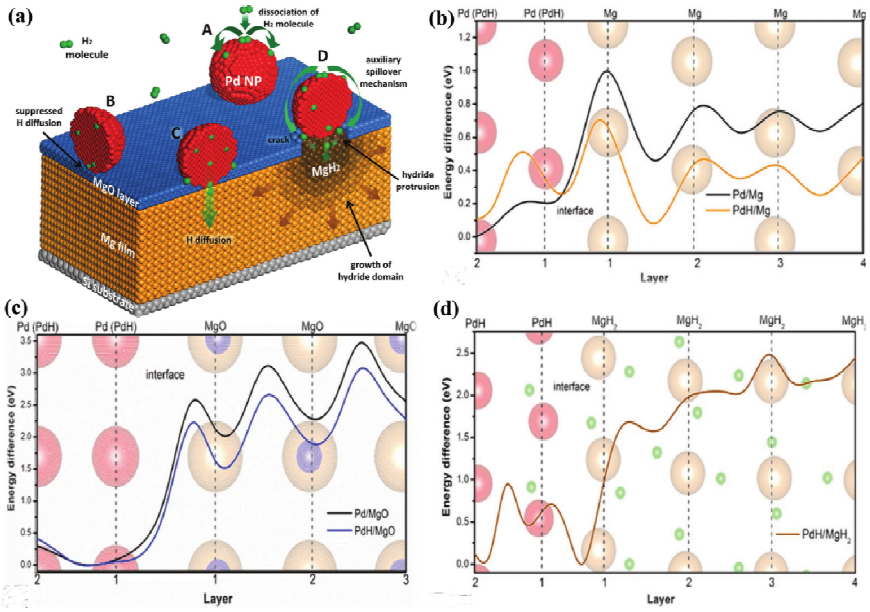

Figure 5. *(a) Schematic summary of hydrogenation mechanism of a surface-oxidized Mg film through Pd nanoparticles, energy barriers for hydrogen diffusion perpendicular to (b) Pd(H)-Mg, (c) Pd(H)-MgO, and (d) PdH-MgH_2 interfaces [91]. Reproduced with permission from [91], copyright 2017 John Wiley and Sons.*

3.4 Hydrogen release from MgH_2

3.4.1 Substitution and light element presence in the interstitial site at the MgH_2 surface

Calculations showed that Nb was the best substitution element used as doping among Sc, Ti, V, Cr, Y, Zr, Nb, and Mo [92] for hydrogen release. This was mainly because Nb substitution in MgH_2 could induce a magnetic moment, which facilitated the formation of spin-down donors and spin-up acceptors. By studying the transition level energies of H vacancies, Mg vacancies, and H-Mg divacancies, they found that hydrogen vacancies were the dominant defect and that V_H^+ diffused more readily than V_H^0 with states near the Fermi level filled. The addition of Nb vacancies can elongate

the Mg-H bond, thereby leading to enhanced hydrogen desorption properties [93]. Comparing with the electronic structure and dopant occupation energy calculations of the Nb atom in the interstitial location, Nb preferred to occupy the substitutional site. The neighbouring hydrogen vacancies were easier to generate in the doped MgH_2 system [94]. Khatabi *et al.* found that the co-substitution of Li and Zn resulted in excellent thermodynamic improvement compared to pure and single substitutions in MgH_2. The activation energy of $Mg_{14}LiZnH_{32}$ was also decreased significantly in comparison to that of pure MgH_2 and those with single substitutions of Zn and Ti. Kinetic Monte Carlo simulation curves for desorption showed that the double substitution of MgH_2 not only improved its thermodynamics but also enhanced its sorption kinetics [95,96]. V and Mn substitutions in Mg_9H_{18} clusters can also decrease the decomposition temperature [97]. By using the Satava-Sestak method, the desorption activation energy of Fe-atom-incorporated β-MgH_2 was calculated to be 110.3 kJ mol^{-1}. The incorporated Fe and Ni would form atomic clusters FeH_4/FeH_2 [98] and Ni/NiH_4 [99] that facilitate electron transfer from the H anion to the Fe atom, thereby leading to the moderate strength of the electron attractions of Fe-H and Ni-H. In another study, Fe and Ti co-substitution was found to be more energetically favourable than single-substitution of Ti or Fe in the surface, and the co-substitution was useful for decreasing the H, Mg and complex Mg-H vacancy formation energies [100]. Studies showed that the Cu dopant on MgH_2 (001) and (110) surfaces preferred to occupy the interstitial site rather than substitute a Mg atom and formed a CuH_4 cluster with H ions. The Cu-Mg and Cu-H interactions strongly weakened the Mg-H

interactions and thus the dehydrogenation temperature can be reduced [101]. The Pd atom that was adsorbed on the MgH_2 (110) surface also decreased the hydrogen release energy barrier from 1.802 eV to 1.154 eV [102].

To increase the hydrogen storage capacity of MgH_2, interstitial C, N and/or B light elements were added to MgH_2, and the interactions with H calculations were designed [103-107]. Wu *et al.* investigated the influence of B doping on the dehydrogenation kinetics and thermodynamic properties of MgH_2. They found that metalloid B doping decreased the dehydrogenation energy and the desorption temperature and mitigated the reduction of the thermal stability for Mg-based systems [108]. In contrast to the conventional belief that MgO prevents the dehydrogenation of MgH_2, calculations showed that the thin MgO and/or transition metal dissolved Mg(TM)O [109,110] layers weakened the Mg-H bond and that hydrogen can diffuse outside the Mg surface. However, the thickness of the MgO layer should be an important factor for the dehydrogenation kinetics.

3.4.2 Strain effect on hydrogen release from MgH_2

The strain of the Mg particles in the synthesis process may influence the hydrogen storage performance; thus, calculations have been conducted in recent years. Tang *et al.* reported that the elastic effects and relative positions strongly affected the incoherent interface stabilities by influencing the incoherent interfacial structure, and strain strongly facilitated defect formation [111]. The biaxial strain on MgH_2 can weaken the structural stability and decrease the hydrogen desorption enthalpy and the dehydrogenation temperature. The effect of tensile strain for improving the

dehydrogenation thermodynamics was superior to that of compressive strain [112,113]. Further studies showed that the hydrogen desorption enthalpy decreased substantially with increasing strain due to the induced energy gap of MgH_2 [114]. The interface formation energies for MgH_2 that epitaxially contacted TiH_2 were strongly favourable, and the strain that was induced by TiH_2 (111) on MgH_2 can reduce the dehydrogenation enthalpy [115]. Therefore, the introduction of a small amount of strain in the preparation process may play a vital role in the enthalpy decrease, similaring to those of the nanoscale calculations that are discussed in previous sections.

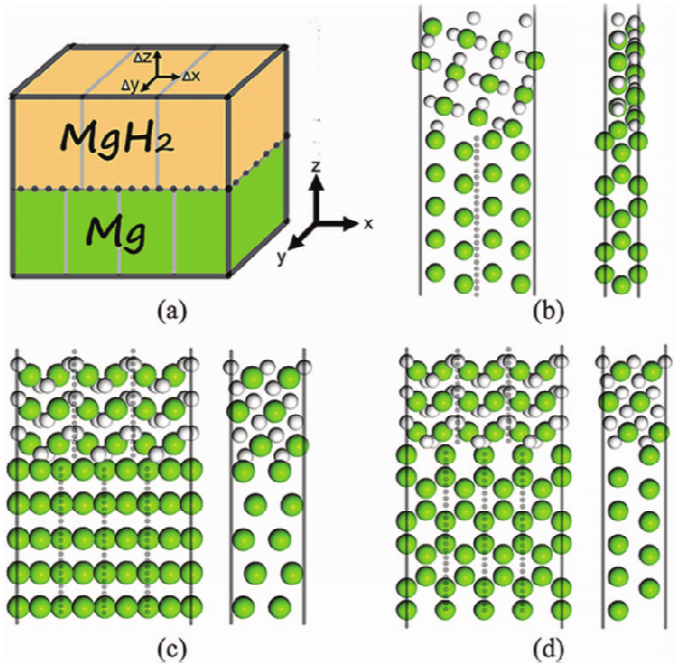

Figure 6. *(a) Front and side views of supercells of interfaces for (b) Mg(10$\bar{1}$0)/MgH_2 (210), (c) Mg(0001)/MgH_2 (101) and (d) Mg(10$\bar{1}$0)/MgH_2 (101) [111]. Reproduced with permission from [111], copyright 2014 AIP Publishing.*

3.4.3 Interaction of hydrogen with decorated catalyst particles

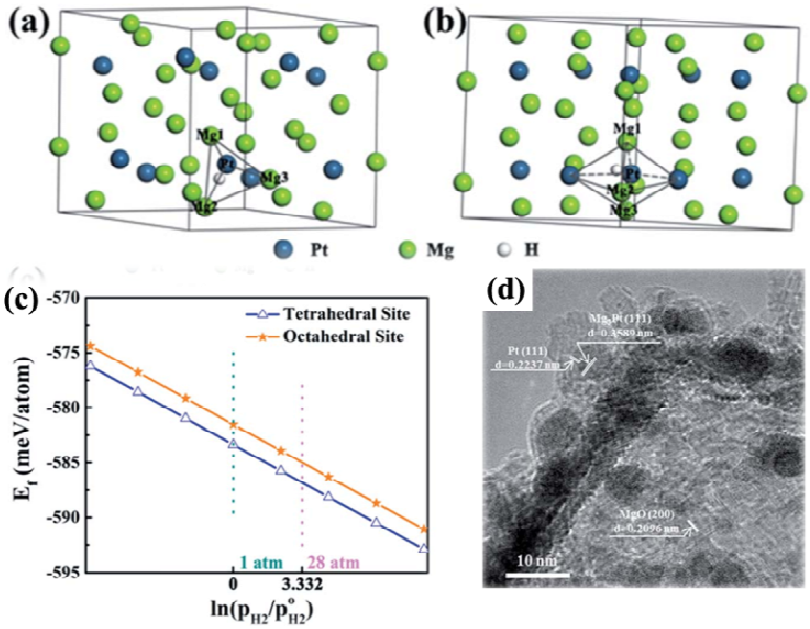

Figure 7. *Theoretical calculation results for the Mg@Pt composite. Interstitial hydrogen atom (a) in the tetrahedral sites, (b) in the octahedral sites of Mg_3Pt, (c) defect formation energy of H atom dependence on hydrogen pressure at the tetrahedral and octahedral site, (d) TEM image of the Mg@Pt composite [116]. Reproduced with permission from [116], copyright 2019 Royal Society of Chemistry.*

The calculation results of interactions of hydrogen molecules/atoms with Mg clusters, Mg slabs and interfaces are used mainly as guidance and explanations for experimental phenomena. Therefore, the interaction calculations of hydrogen with decorated catalyst particles are important for better understanding the micro-mechanism. Zou *et al.* studied the occupation behaviour of hydrogen atoms in interstitial sites. They found that the defect formation energies for tetrahedral and octahedral sites decreased with increasing hydrogen partial pressure. The calculation results also implied that the H doping weakened the bonds between the metal atoms.

Hence, the H-stabilized Mg_3Pt can be treated as a "hydrogen pump" for transferring H atoms during the dehydrogenation process, see Fig. 7a-7d [116]. The Mg-H bond length for MgH_2 that was adsorbed on the ZrCo (110) surface was dramatically increased to 3.844 Å, which is much longer than that of pristine MgH_2 (1.716 Å), implying that the catalytic effects of ZrCo particles are effective [61]. Liu *et al.* constructed Nb-O and Nb-N-O clusters that were adsorbed on the MgH_2 (110) surface model, which described the addition of N-Nb_2O_5 to the MgH_2 system (see Fig. 8a). The authors found that the presence of Nb-O and Nb-N-O clusters induced the distortion of MgH_2 after structural relaxation (see Fig. 8b-e). The increased bond length of Mg-H in Fig. 8b-c indicated that the clusters can weaken the stability of MgH_2. Moreover, the presence of N showed a positive effect on the contribution of Nb in the DOS around the Fermi level [117], see Fig. 8f. Compared to the formation energies of hydrogen vacancies in MgH_2 and $CeH_{2.73}$, the *ab initio* calculation results demonstrated that the formation energy in the $CeH_{2.73}/CeO_2$ boundary region was significantly reduced [118], which benefited from the raised Fermi level of MgH_2 for the oxygen vacancies that provided electrons to the Fermi level of the system [119]. These results demonstrated that due to the interfacial effect of $CeH_{2.75}/CeO_2$, it could be served as an efficient hydrogen pump. The calculated binding energies for MgH_2 that was adsorbed on the NiPc and NbTi surfaces were increased [120, 121], which can describe the high aggregation resistance of the NiPc particles. The increased electron transfer between NiPc and MgH_2 and the increased ability of Nb atoms to donate electrons to H atoms that were caused by electron redistribution in NbTi

clusters led to the weakened bond strength of Mg-H.

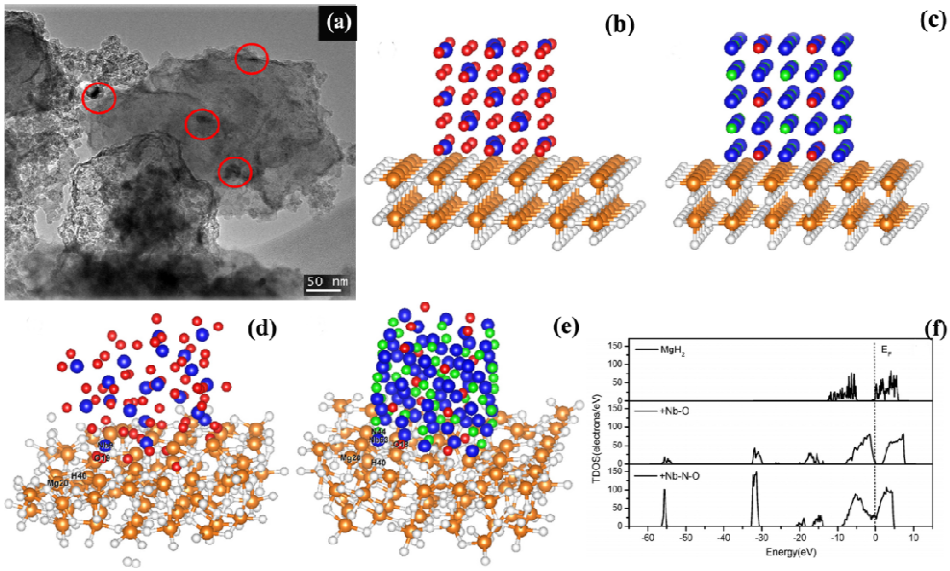

Figure 8. (a) *TEM image of MgH_2/*N-Nb_2O_5 composite, *the initial (b) Nb-O, (c) Nb-N-O and calculated (d) Nb-O, (e) Nb-N-O clusters on the MgH_2 (110) face, (f) DOS of the MgH_2 (110) crystal face, Nb-O and Nb-N-O doped MgH_2. Color codes: white is hydrogen, orange is Mg, blue is Nb, red is O and green is N [117]. Reproduced with permission from [117], copyright 2019 Elsevier.*

3.5 Influence of the particle size on the hydrogen storage performance

Experimental studies show that the Mg-H bond energies are affected by the particle size and that the thermodynamic properties can be improved for Mg nanoparticles of approximately 5-20 nm [46]. Moreover, the carbon confined materials showed positive effects on the decreased thermodynamic stability [38-40,122]. To identify the influence of the particle size on the dynamic performance, calculations on Mg clusters were conducted via DFT methods. The calculated results showed that the desorption energy for Mg_nH_{nx} was significantly decreased to

approximately 50 KJ mol^{-1} for n>6 and x=2. This was in full agreement with experimental evidence for colloidal MgH_2 particles of 5 nm [123]. Buckley *et al.* calculated the enthalpy differences of Mg_nH_{2n} clusters with various particle sizes and found that the desorption energy decreased with increasing particle size, which was contrary to the experimental results [124]. The computational calculations of MgH_2 particles of 1-2 nm showed that charge transfer to the carbon scaffold played a critical role in the observed low-temperature dehydrogenation [125]. Vajeeston *et al.* suggested that a particle size for MgH_2 of 2.2 nm was the key point for desorption energy and it was easier for removal of hydrogen from the centre of the scaffold than that from bulk MgH_2 [126]. However, a deep study of the differences in dehydrogenation activation energies should be conducted, and the main factors for the formation of pure MgH_2 clusters with various sizes should be clarified.

4. Conclusions and outlook

The following applications of density-functional-theory-based first-principles calculations were summarized: the structural stability of the pure Mg and transition metal-doped MgH_2 materials, the hydrogen site preferences in these surfaces and the interfaces of Mg/alloys; identification of the effects of doping and strain on the diffusion pathway and diffusion energies at the Mg(0001) and high indexed Mg($10\bar{1}3$) surfaces; NEB calculations of the dissociation energies of hydrogen molecules on pure Mg surfaces and interfaces of Mg/catalyst; the hydrogen adsorption attitudes on surfaces; the effects of element doping and substitution on the dehydrogenation of MgH_2; and examination of the strain effects on the stability of Mg-H bands. The strain

effect calculations were conducted mainly on established supercells via the incorporation of strain into the calculation process, which represented the Mg/MgH_2 surface, element-doped Mg and/or MgH_2, and MgH_2 clusters. Particle size effect calculations were focused mainly on pure and/or element-doped Mg/MgH_2 clusters (typically below 50 atoms) rather than interfaces. The catalytic effects were examined mainly for single-element-doped Mg(MgH_2) slabs, alloy/Mg(MgH_2) slabs, and combinations of alloy clusters that were absorbed on Mg(MgH_2) slabs. In addition to the calculation results that are summarized above, the following issues may be further considered in the future:

(1) Although the hydrogen diffusion paths of hydrogen atoms onthe surface of pure Mg and Mg(0001)-catalyzed by metal and alloy catalyst slabs have been calculated, reasonable calculations for hydrogen dissociation at these interfaces can be conducted in future studies. The stabilities of MgH_2-metal and alloy catalyst slabs and the hydrogen vacancy formation energies and biaxial strain effects should be clarified for further investigation of the dehydrogenation performance of MgH_2.

(2) The calculated strain showed positive effects on the dehydrogenation of MgH_2. However, the MgH_2/catalyst mismatch should be considered in future calculations, and the strains from other dimensions and the strains on the Mg(MgH_2)-metal and alloy catalyst interfaces require further calculations.

(3) Experiments results demonstrate that metals and alloys exert satisfactory catalytic effects on dehydrogenation. However, the effects of metal and alloy clusters rather than atom doping on the stability of MgH_2 and the interactions with Mg-H bonds

should be calculated in the future to better describe the catalytic mechanism.

Acknowledgement

This work was supported by research program of National Natural Science Foundation of China (51731002), the Key Laboratory of Biomedical Effects of Nanomaterials and Nanosafety, Chinese Academy of Sciences (No: NSKF201908), Youth Top Talent Foundation of Yantai University (2219008) and Top Discipline in Materials Science of Shandong Province.

References

[1] Liu JJ, Cheng HH, Han SM, Liu HF, Huot J. Hydrogen storage properties and cycling degradation of single-phase $La_{0.60}R_{0.15}Mg_{0.25}Ni_{3.45}$ alloys with A_2B_7-type superlattice structure. Energy 2020;192:116617.

[2] Yasuoka S, Ishida J, Kishida K, Inui H. Effects of cerium on the hydrogen absorption-desorption properties of rare earth-Mg-Ni hydrogen-absorbing alloys. J Power Sources 2017;346:56-62.

[3] Chen XY, Chen RR, Ding X, Fang HZ, Li XZ, Ding HS, Su YQ, Guo JJ, Fu HZ. Effect of phase formation on hydrogen storage properties in Ti-V-Mn alloys by zirconium substitution. Energy 2019;166:587-97.

[4] Galey B, Auroux A, Etienne SS, Grellier M, Dhaher S, Postole G. Impact of the addition of poly-dihydrogen ruthenium precursor complexes on the hydrogen storage properties of the Mg/MgH_2 system. Sustain. Energy Fuels 2018;2:2335-44.

[5] Wang YQ, Lan ZQ, Huang XT, Liu HZ, Guo J. Study on catalytic effect and mechanism of MOF (MOF=ZIF-8, ZIF-67, MOF-74) on hydrogen storage properties

of magnesium. Int. J. Hydrogen Energy 2019;44:28863-73.

[6] Zhang JG, Zhu YF, Lin HJ, Liu YN, Zhang Y, Li SY, Ma ZL, Li LQ. Metal hydride nanoparticles with ultrahigh structural stability and hydrogen storage activity derived from microencapsulated nanoconfinement. Adv. Mater. 2017;29:1700760.

[7] Zhang XL, Liu YF, Zhang X, Hu JJ, Gao MX, Pan HG. Empowering hydrogen storage performance of MgH_2 by nanoengineering and nanocatalysis. Mater. Today Nano 2020;9:100064.

[8] Zhang LT, Ji L, Yao ZD, Yan NH, Sun Z, Yang XL, Zhu XQ, H SLu, Chen LX. Facile synthesized Fe nanosheets as superior active catalyst for hydrogen storage in MgH_2. Int. J. Hydrogen Energy 2019;44:21955-64.

[9] Galey B, Auroux A, Sylviane SE, Dhaher S, Grellier M, Postole G. Improved hydrogen storage properties of Mg/MgH_2 thanks to the addition of nickel hydride complex precursors, Int. J. Hydrogen Energy 2019;44:28848-62.

[10] Chen M, Hu MM, Xie XB, Liu T. High loading nanoconfinement of V-decorated Mg with 1 nm carbon shells: hydrogen storage properties and catalytic mechanism. Nanoscale 2019;11:10045-55.

[11] Huang X, Xiao XZ,Wang XC , Wang CT, Fan XL, Tang ZC, Wang CY, Wang QD, Chen LX. Synergistic catalytic activity of porous rod-like $TMTiO_3$ (TM =Ni and Co) for reversible hydrogen storage of magnesium hydride. J. Phys. Chem. C 2018;122:27973-82.

[12] Liu P, Lian JJ, Chen HP, Liu XJ, Chen YL, Zhang TH, Yu H, Lu GJ, Zhou SX. In-situ synthesis of Mg_2Ni-Ce_6O_{11} catalyst for improvement of hydrogen storage in

magnesium. Chem. Eng. J. 2020;385:123448.

[13] Noritake T, Towata S, Aoki M, Seno Y, Hirose Y, Nishibori E, Takata M, Sakata M. Charge density measurement in MgH_2 by synchrotron X-ray diffraction. J. Alloys Compd. 2003;356-357:84-6.

[14] Bastide JP, Bonnetot B, Létoffé JM, Claudy P. Polymorphisme de l'hydrure de magnesium sous haute pression. Mat. Res. Bull. 1980; 15:1779-87.

[15] Luo Q, Li JD, Li B, Liu B, Shao HY, Li Q. Kinetics in Mg-based hydrogen storage materials: Enhancement and Mechanism. J. Magnes. Alloys 2019;7:58-71.

[16] Lobo N, Takasaki A, Mineo K, Klimkowicz A, Goc K. Stability investigation of the γ-MgH_2 phase synthesized by high-energy ball milling. Int. J. Hydrogen Energy 2019;44:29179-88.

[17] Kitabayashi K, Edalati K, Li HW, Akiba E, Horita ZJ. Phase Transformations in MgH_2-TiH_2 hydrogen storage system by high-pressure torsion process. Adv. Energy Mater. 2020;22:1900027.

[18] Czujko T, Varin RA, Chiu C, Wronski Z. Investigation of the hydrogen desorption properties of Mg+10wt.%X (X=V, Y, Zr) submicrocrystalline composites. J. Alloys Compd. 2006;414:240-7.

[19] Gao SC, Wang XH, Liu HZ, He T, Wang YY, Li SQ, Yan M. Effects of nano-composites (FeB, FeB/CNTs) on hydrogen storage properties of MgH_2. J. Power Sources 2019;438:227006.

[20] Liu T, Zhang TW, Qin CG, Zhu M, Li XG. Improved hydrogen storage properties of Mg-V nanoparticles prepared by hydrogen plasma-metal reaction. J. Power Sources

2011;196:9599-604.

[21] Bhatnagar A, Pandey SK, Vishwakarma AK, Singh S, Shukla V, Soni PK, Shaz MA, Srivastava ON. Fe_3O_4@graphene as a superior catalyst for hydrogen de/absorption from/in MgH_2/Mg. J. Mater. Chem. A 2016;4:14761-72.

[22] Zhang YP, Shen YH, Xie XB, Du W, Kang LT, Wang Y, Sun XQ, Li ZH, Wang B, One-step synthesis of the reduced graphene oxide@NiO composites for supercapacitor electrodes by electrode-assisted plasma electrolysis, Mater. Des. 2020;196:109111.

[23] Xie XB, Ni C, Lin ZH, Wu D, Sun XQ, Zhang YP, Wang B, Du W, Phase and morphology evolution of high dielectric CoO/Co_3O_4 particles with CoO nanoneedles on surface for excellent microwave absorption application. Chem. Eng. J. 2020;396:125205.

[24] Alsabawi K, Mac A, Gray E, Webb CJ. The effect of ball-milling gas environment on the sorption kinetics of MgH_2 with/without additives for hydrogen storage. Int. J. Hydrogen Energy 2019;44:2976-80.

[25] Liu YF, Du HF, Zhang X, Yang YX, Gao MX, Pan HG. Superior catalytic activity derived from a two-dimensional Ti_3C_2 precursor towards the hydrogen storage reaction of magnesium hydride. Chem. Commun. 2016;52:705-8.

[26] Hu MM, Xie XB, Chen M, Zhu CX, Liu T. TiC_X-decorated Mg nanoparticles confined in carbon shell: Preparation and catalytic mechanism for hydrogen storage. J. Alloys Compd. 2020;817:152813.

[27] Soni PK, Bhatnagar A, Shaz MA, Srivastava ON. Effect of graphene templated

fluorides of Ce and La on the de/rehydrogenation behavior of MgH_2. Int. J. Hydrogen Energy 2017;42:20026-35.

[28] Youn JS, Phan DT, Park CM, Jeon KJ. Enhancement of hydrogen sorption properties of MgH_2 with a MgF_2 catalyst. Int. J. Hydrogen Energy 2017;42:20120-4.

[29] Ismail M, Halim Yap FA, Sulaiman NN, Ishak MHI. Hydrogen storage properties of a destabilized MgH_2-Sn system with TiF_3 addition. J. Alloys Compd. 2016;678:297-303.

[30] Yuan ZM, Zhang BW, Zhang YH, Guo SH, Dong XP, Zhao DL. A comparison study of hydrogen storage properties of as-milled Sm_5Mg_{41} alloy catalyzed by CoS_2 and MoS_2 nano-particles. J. Mater. Sci. Technol. 2018;34:1851-8.

[31] Xie XB, Ma XJ, Liu P, Shang JX, Li XG, Liu T. Formation of multiple-phase catalysts for the hydrogen storage of Mg nanoparticles by adding flowerlike NiS. ACS Appl. Mater. Interfaces 2017;9:5937-46.

[32] Liu P, Xie XB, Xu L, Li XG, Liu T. Catalytic effect of $(Ti_{0.85}Zr_{0.15})_{1.05}Mn_{1.2}Cr_{0.6}V_{0.1}Cu_{0.1}$ on hydrogen storage properties of ultrafine magnesium particles. RSC Adv. 2017;7:34538-47.

[33] El-Eskandarany MS, Shaban E, Alsairafi AA. Synergistic dosing effect of TiC/FeCr nanocatalysts on the hydrogenation/dehydrogenation kinetics of nanocrystalline MgH_2 powders. Energy 2016;104:158-70.

[34] Liu T, Cao YR, Qin CG, Li XG. Synthesis and hydrogen storage properties of Mg-10.6La-3.5Ni nanoparticles. J. Power Sources 2014;246:277-82.

[35] Xie XB, Chen M, Liu P, Shang JX, Liu T. High hydrogen desorption properties

of Mg-based nanocomposite at moderate temperatures: The effects of multiple catalysts in situ formed by adding nickel sulfides/grapheme. J. Power Sources 2017; 371:112-8.

[36] Xie XB, Chen M, Liu P, Shang JX, Liu T. Synergistic catalytic effects of the Ni and V nanoparticles on the hydrogen storage properties of Mg-Ni-V nanocomposite. Chem. Eng. J. 2018;347:145-55.

[37] Xie XB, Chen M, Hu MM, Liu T. Recoverable Ni_2Al_3 nanoparticles and their catalytic effects on Mg-based nanocomposite during hydrogen absorption and desorption cycling. Int. J. Hydrogen Energy 2018;43:21856-63.

[38] Liu YN, Zou JX, Zeng XQ, Wu XM,.Tian HY, Ding WJ, Wang L, Walter A. Study on hydrogen storage properties of Mg nanoparticles confined in carbon aerogels. Int. J. Hydrogen Energy 2013;38:5302-8.

[39] Au YS, Obbink MK, Srinivasan S, Magusin PCMM,.de Jong KP, de Jongh PE. The size dependence of hydrogen mobility and sorption kinetics for carbon-supported MgH_2 particles. Adv. Funct. Mater. 2014;24:3604-11.

[40] Nielsen TK, Manickam K, Hirscher M, Besenbacher F, Jensen TR. Confinement of MgH_2 nanoclusters within nanoporous aerogel scaffold materials. ACS Nano 2009;3:3521-8.

[41] Yao XD, Wu CZ, Du AJ, Zou J, Zhu ZH, Wang P, Cheng HM, Smith S, Lu GQ. Metallic and carbon nanotube-catalyzed coupling of hydrogenation in magnesium. J. Am. Chem. Soc. 2007;129:15650-4.

[42] Wagemans RWP, Lenthe JH, Jongh PE, Dillen AJ, Jong KP. Hydrogen storage in

magnesium clusters: Quantum chemical study. J. Am. Chem. Soc. 2005;127:16675-80.

[43] Wu Z, Allendorf MD, Grossman JC. Quantum monte carlo simulation of nanoscale MgH_2 cluster thermodynamics. J. Am. Chem Soc. 2009;131:13918-9.

[44] Li LL, Peng B, Ji WQ, Chen J. Studies on the hydrogen storage of magnesium nanowires by density functional theory. J. Phys. Chem. C 2009;113:3007-13.

[45] Hevia E, Mulvey RE. A record-breaking magnesium hydride molecular cluster: implications for hydrogen storage. Angew. Chem. Int. Ed. 2011;50:9242-3.

[46] Norberg NS, Arthur TS, Fredrick SJ, Prieto AL. Size-dependent hydrogen storage properties of Mg nanocrystals prepared from solution. J. Am. Chem Soc. 2011;133:10679-81.

[47] Cho ES, Ruminski AM, Aloni S, Liu YS, Guo JH, Urban JJ. Graphene oxide/metal nanocrystal multilaminates as the atomic limit for safe and selective hydrogen storage. Nat. Commun. 2016;7:10804.

[48] Xia GL, Tan YB, Chen XW, Sun DL, Guo ZP, Liu HK, Ouyang LZ, Zhu M, Yu XB. Monodisperse magnesium hydride nanoparticles uniformly self-assembled on graphene. Adv. Mater. 2015;27:5981-8.

[49] Wu YN, Li XT, Chen ZJ, Yu JS, Qiu SB, Yang XB, Zhao YJ. Mg-X(X=Ni,Pd,Ti,Nb) interface and atomic mixture effect:a first-principles study. Mater. Res. Express 2019;6:016305.

[50] Edalati K, Kitabayashi K, Ikeda Y, Matsuda J, Li HW, Tanaka I, Akiba E, Horita Z. Bulk nanocrystalline gamma magnesium hydride with low dehydrogenation

temperature stabilized by plastic straining via high-pressure torsion. Scr. Mater. 2018;157:54-7.

[51] Wang QQ, Kong XG, Han HL, Sang G, Zhang GH, Gao T. Effect of doping Hf on the hydrogen dissociation and diffusion mechanism on the ZrCo (110) surface. Appl. Surf. Sci. 2019;483:383-90.

[52] Blöchl PE. Projector augmented-wave method. Phys. Rev. B 1994;50:17953.

[53] Perdew JP, Burke K, Ernzerhof M. Generalized gradient approximation made simple. Phys. Rev. Lett. 1996;77:3865-8.

[54] Jones RO, Gunnarsson O. The density functional formalism: its applications and prospects. Rev. Mod. Phys. 1989;61:689-746.

[55] Monkhorst HJ, Pack JD. Special points for Brillouin-zone integrations. Phys. Rev. B 1976;13:5188.

[56] Henkelman G, Uberuaga BP, Jonsson H. A climbing image nudged elastic band method for finding saddle points and minimum energy paths. J. Chem. Phys. 2000;113:9901-4.

[57] Henkelman G, Jonsson H. Improved tangent estimate in the nudged elastic band method for finding minimum energy paths and saddle points. J. Chem. Phys. 2000;113:9978-85.

[58] Wu Z, Yang FS, Bao ZW, Nyamsi SN, Zhang ZX. Improvement in hydrogen storage characteristics of Mg-based metal hydrides by doping nonmetals with high electronegativity: A first-principle study. Comp. Mater. Sci. 2013;78:83-90.

[59] Segall MD, Lindan PJD, Probert MJ, Pickard CJ, Hasnip PJ, Clark SJ.

First-principles simulation: ideas, illustrations and the CASTEP code. J. Phys.: Condens. Matter 2002;14:2717-44.

[60] Eroglu E, Aydin S, Simsek M. Effect of boron substitution on hydrogen storage in Ca/DCV graphene: A first-principle study. Int. J. Hydrogen Energy 2019;44:27511-28.

[61] Zhang LT, Cai ZL, Zhu XQ, Yao ZD, Sun Z, Ji L, Yan NH, Xiao BB, Chen LX. Two-dimensional ZrCo nanosheets as highly effective catalyst for hydrogen storage in MgH_2. J. Alloys Compd. 2019;805:295-302.

[62] Xie XB, Li YC, Chen M, Hu MM, Feng YX, Shang JX, Liu T. Catalytic effects of decorating AlV_3 nanocatalyst on hydrogen storage performance of $Mg@Mg_{17}Al_{12}$ nanocomposite: experimental and theoretical study. ACS Sustainable Chem. Eng. 2020;8:4920-30.

[63] Vegge T. Locating the rate-limiting step for the interaction of hydrogen with Mg(0001) using density-functional theory calculations and rate theory. Phys. Rev. B 2004;70:035412.

[64] Wang ZW, Guo XJ, Wu MY, Sun Q, Jia Y. First-principles study of hydrogen dissociation and diffusion on transition metal-doped Mg(0001) surfaces. Appl. Surf. Sci. 2014;30:40-5.

[65] Xin JH, Wang JC, Du Y, Sun LX, Huang BY. Site preference and diffusion of hydrogen during hydrogenation of Mg: A first-principles study. Int. J. Hydrogen Energy 2016;41:3508-16.

[66] Du AJ, Smith SC, Yao XD, Lu GQ. The role of Ti as catalyst for the dissociation

of hydrogen on a Mg(0001) surface. J. Phys. Chem. B 2005;109:18037.

[67] Pozzo M, Alfe D, Amieiro A, French S, Pratt A. Hydrogen dissociation and diffusion on Ni- and Ti-doped Mg(0001) surfaces. J. Chem. Phys. 2008;128:094703.

[68] Wu GX, Zhang JY, Wu YQ, Li Q, Chou KC, Bao XH. Density functional theory study of hydrogenation mechanism in Fe-doped Mg(0001) surface. Appl. Surf. Sci. 2009;255:6338.

[69] Chen M, Yang XB, Cui J, Tang JJ, Gan LY, Zhu M, Zhao YJ. Stability of transition metals on Mg(0001) surfaces and their effects on hydrogen adsorption. Int. J. Hydrogen Energy 2012;37:309.

[70] Tang JJ, Yang XB, Chen M, Zhu M, Zhao YJ. First-principles study of biaxial strain effect on hydrogen adsorbed Mg (0001) surface. J. Phys. Chem. C 2012;116:14943-9.

[71] He C, Chen YL, Sheng Y. First-principles study of molecular hydrogen adsorption on Mg_nZr (n=1~11) clusters. Eur. Phys. J. D 2019;73:90.

[72] Dai JH, Xie RW, Chen YY, Song Y. First principles study on stability and hydrogen adsorption properties of Mg/Ti interface. Phys. Chem. Chem. Phys. 2015;17:16594-16600.

[73] Chen YY, Dai JH, Song Y. Stability and hydrogen adsorption properties of Mg/Mg_2Ni interface: A first principles study. Int. J. Hydrogen Energy 2018;43;16598-608.

[74] Dai JH, Song Y, Shi B, Yang R. First-principles study on a potential hydrogen storage medium of Mg/TiAl sandwiched films. J. Phys. Chem. C 2013;117:25374-80.

[75] Dai JH, Jiang XW, Song Y. Stability and hydrogen adsorption properties of $Mg/TiMn_2$ interface by first principles calculation. Surf. Sci. 2016;653:22-6.

[76] Zhou CS, Fang ZZ, Ren C, Li JZ, Lu J. Effect of Ti intermetallic catalysts on hydrogen storage properties of magnesium hydride. J. Phys. Chem. C 2013;117:12973-80.

[77] Bhatnagar A, Johnson JK, Shaz MA, Srivastava ON. TiH_2 as a dynamic additive for improving the de/rehydrogenation properties of MgH_2: A combined experimental and theoretical mechanistic investigation. J. Phys. Chem. C 2018;122:21248-61.

[78] Chen HP, Ma NN, Li JQ, Wang YJ, She CX, Zhang Y, Li XN, Liu JQ, Feng X, Zhou SX. Effect of atomic iron on hydriding reaction of magnesium: Atomic-substitution and atomic-adsorption cases from a density functional theory study. Appl. Surf. Sci. 2020;504:144489.

[79] Han ZY, Chen HP, Zhou SX. Dissociation and diffusion of hydrogen on defect-free and vacancy defective Mg (0001) surfaces: A density functional theory study. Appl. Surf. Sci. 2017;394:371-7.

[80] Lei HP, Wang CZ, Yao YX, Wang YG, Hupalo M, McDougall D, Tringides M, Ho K. Strain effect on the adsorption, diffusion, and molecular dissociation of hydrogen on Mg (0001) surface. J. Chem. Phys. 2013;139:224702.

[81] Ye JH, Zhao YJ, Fang YX, Lin HJ, Bai L, Tang JJ. Hydrogen adsorption, dissociation, and diffusion on high-index Mg(1013) and their comparisons with Mg(0001): A systematic first-principles study. Int. J. Hydrogen Energy 2019;44:4897-906.

[82] Banerjee S, Pillai CGS, Majumder C. Dissociation and diffusion of hydrogen on the Mg(0001) surface: catalytic effect of V and Ni double substitution. J. Phys. Chem. C 2009;113:10574-9.

[83] Chen M, Cai ZZ, Yang XB, Zhu M, Zhao YJ. Theoretical study of hydrogen dissociation and diffusion on Nb and Ni co-doped Mg(0001): A synergistic effect. Suf. Sci. 2012;606:L45-9.

[84] Liu BG, Zhang B, Wu Y, Lv W, Zhou SX. Theoretical prediction and experimental study on catalytic mechanism of incorporated Ni for hydrogen absorption of Mg. Int. J. Hydrogen Energy 2019;44:27885-95.

[85] Li YF, Yang Y, Sun B, Song HZ, Wei YH, Zhang P. Rotation of hydrogen molecules during the dissociative adsorption on the Mg(0001) surface: a first-principles study. Chin. Phys. B 2010;195:058201.

[86] Wang ZY, Zhao YJ. Role of metal impurity in hydrogen diffusion from surface into bulk magnesium: A theoretical study. Phys. Lett. A 2017;381:3696-700.

[87] Ouyang LZ, Tang JJ, Zhao YJ, Wang H, Yao XD, Liu JW, Zou J, Zhu M. Express penetration of hydrogen on Mg(1013) along the close-packed-planes. Sci. Rep. 2015;5:10776.

[88] Shervani S, Mukherjee P, Gupta A, Mishra G, Illath K, Ajithkumard TG, Sivakumar S, Sen P, Balani K, Subramaniam A. Multi-mode hydrogen storage in nanocontainers. Int. J. Hydrogen Energy 2017;42:24256-62.

[89] Li Q, Li Y, Liu B, Lu XG, Zhang TF, Gu QF. The cycling stability of the in situ formed Mg-based nanocomposite catalyzed by YH_2. J. Mater. Chem. A

2017;5:17532-43.

[90] Luo Q, Gu QF, Liu B, Zhang TF, Liu WQ, Li Q. Achieving superior cycling stability by in situ forming NdH_2-Mg-Mg_2Ni nanocomposites. J. Mater. Chem. A 2018;6:23308-17.

[91] Kumar S, Pavloudis T, Singh V, Nguyen H, Steinhauer S, Pursell C, Clemens B, Kioseoglou J, Grammatikopoulos P, Sowwan M. Hydrogen flux through size selected Pd nanoparticles into underlying Mg nanofilms. Adv. Energy Mater. 2018;8:1701326.

[92] El Khatabi M, Bhihi M, Naji S, Labrim H, Benyoussef A, El Kenz A, Loulidi M. Study of doping effects with 3d and 4d-transition metals on the hydrogen storage properties of MgH_2. Int. J. Hydrogen Energy 2016;41:4712-8.

[93] Gaztañaga F, Luna CR, Orazi V, González E, Faccio R, Jasen P. Effects of native vacancies on Nb-doped MgH_2 using density functional theory calculations. J. Phys. Chem. C 2018;122:27955-62.

[94] German E, Gebauer R. Improvement of hydrogen vacancy diffusion kinetics in MgH_2 by niobium and zirconium-doping for hydrogen storage applications. J. Phys. Chem. C 2016;120:4806-12.

[95] El Khatabi M, Bhihi M, Lakhal M, Abdellaoui M, Benyoussef A, El Kenz A, Loulidi M. Enhanced hydrogen sorption kinetics of co-doped MgH_2 hydrides. Comp. Mater. Sci. 2018;152:192-5.

[96] Bhihi M, El Khatabi M, Lakhal M, Naji S, Labrim H, Benyoussef A, El Kenz A, Loulidi M. First principal study of hydrogen storage in doubly substituted Mg based hydrides. Int. J. Hydrogen Energy 2015;40:8356.

[97] Gong X, Shao XH. Stability, electronic structure, and dehydrogenation properties of pristine and doped 2D MgH_2 by the first principles study. Metals 2018;8:482.

[98] Chen HP, Yu H, Zhang QQ, Liu BG, Liu P, Zhou XP, Han ZY, Zhou SX. Enhancement in dehydriding performance of magnesium hydride by iron incorporation: A combined experimental and theoretical investigation. J. Power Sources 2016;322:179-86.

[99] Wu Z, Zhu LY, Yang FS, Nyamsi SN, Porpatham E, Zhang ZX. Toward the design of interstitial nonmetals co-doping for Mg-based hydrides as hydrogen storage material. J. Mater. Res. 2018;33;4080-91.

[100] Ri S, Um KJ, Wi JH, Kim JC, Kim NH. Effects of singlee and co-substitution of Ti and Fe on vacancy formation and dehydrogenation from MgH_2 (110) surface: Ab initio study. Int. J. Hydrogen Energy 2019;9:22761.

[101] Matar SF. Light elements-induced iono-covalent character in MgH_2: An ab-initio approach. Comp. Mater. Sci. 2013;69:423-7.

[102] Wu XX, Hu W. First-principles study of Pd single-atom catalysis to hydrogen desorption reactions on MgH_2(110) surface. Chin. J. Chem. Phys. 2019;32:319.

[103] Wu Z, Zhu L, Yang F, Jiang Z, Zhang Z. Influences of interstitial nitrogen with high electronegativity on structure and hydrogen storage properties of Mg-based metal hydride: A theoretical study. Int. J. Hydrogen Energy 2016;41:18550-61.

[104] Zhang J, Yu XF, Mao C, Long CG, Chen J, Zhou DW. Influences and mechanisms of graphene-doping on dehydrogenation properties of MgH_2: Experimental and first-principles studies. Energy 2015;89:957-64.

[105] Wang JJ, Du Y, Sun LX, Li XH. Effects of F and Cl on the stability of MgH_2. Int. J. Hydrogen Energy 2014;39:877-83.

[106] Wu Z, Zhu LY, Yang FS, Jiang Z, Zhang ZX. First-principles insights into influencing mechanisms of metalloid B on Mg-based hydrides. J. Alloys Compd. 2017;693:979-88.

[107] Singh MK, Bhatnagar A, Pandey SK, Mishra PC, Srivastava ON. Experimental and first principle studies on hydrogen desorption behavior of graphene nanofibre catalyzed MgH_2. Int. J. Hydrogen Energy 2017;42:960-8.

[108] Wang HC, Wu DH, Wei LT, Y.ang TB. First-principles investigation of dehydrogenation on Cu-doped MgH_2 (001) and (110) surfaces. J. Phys. Chem. C 2014;118:13607-16.

[109] Zhang J, Yan S, Yu LP, Zhou XJ, Zhou T, Peng P. Enhanced hydrogen storage properties and mechanisms of magnesium hydride modified by transition metal dissolved magnesium oxides. Int. J. Hydrogen Energy 2018;43:21864-73.

[110] Wan LF, Liu YS, Cho ES, Forster JD, Jeong S, Wang HT, Urban JJ, Guo JH, Prendergast D. Atomically thin interfacial suboxide key to hydrogen storage performance enhancements of magnesium nanoparticles encapsulated in reduced graphene oxide. Nano Lett. 2017;17:5540-5.

[111] Tang JJ, Yang XB, Chen LJ, Zhao YJ. Modeling and stabilities of Mg/MgH_2 interfaces: A first-principles investigation. AIP Adv. 2014;4:077101.

[112] Zhang J, Yan S, Qu H. Stress/strain effects on thermodynamic properties of magnesium hydride: A brief review. Int. J. Hydrogen Energy 2017;42:16603-10.

[113] Zhang J, Zhou YC, Ma ZS, Sun LQ, Peng P. Strain effect on structural and dehydrogenation properties of MgH_2 hydride from first-principles calculations. Int. J. Hydrogen Energy 2013;38:3661-9.

[114] Zhang J, Mao C, Chen J, Long CG, Tang K, Zhang MJ, Peng P. Strain tuned dehydrogenation thermodynamics of magnesium based hydride: A first principle study. Comp. Mater. Sci. 2015;105:71-4.

[115] Hao SQ, Sholl DS. Effect of TiH_2 induced strain on thermodynamics of hydrogen release from MgH_2. J. Phys. Chem. C 2012;116:2045-50.

[116] Lu C, Ma YL, Li F, Zhu H, Zeng XQ, Ding WJ, Deng T, Wu JB, Zou JX. Visualization of fast "hydrogen pump" in core-shell nanostructured Mg@Pt through hydrogen-stabilized Mg_3Pt. J. Mater. Chem. A 2019;7:14629-37.

[117] Wang K, Zhang X, Ren ZH, Zhang XL, Hu JJ, Gao MX, Pan HG, Liu YF. Nitrogen-stimulated superior catalytic activity of niobium oxide for fast full hydrogenation of magnesium at ambient temperature. Energy Storage Mater. 2019;23:79-87.

[118] Lin HJ, Tang JJ, Yu Q, Wang H, Ouyang LZ, Zhao YJ, Liu JW, Wang WH, Zhu M. Symbiotic $CeH_{2.73}/CeO_2$ catalyst: A novel hydrogen pump. Nano Energy 2014;9:80-7.

[119] Sharma V, Crozier PA, Sharma R, Adams JB. Direct observation of hydrogen spillover in Ni-loaded Pr-doped ceria. Catal. Today 2012;180:2-8.

[120] Zhang J, Qu H, Yan S, Wu G, Yu XF, Zhou DW. Catalytic effect of nickel phthalocyanine on hydrogen storage properties of magnesium hydride: Experimental

and first-principles studies. Int. J. Hydrogen Energy 2017;42:28485-97.

[121] Wang ZY, Zhang XL, Ren ZH, Liu Y, Hu JJ, Li HW, Gao MX, Pan HG, Liu YF. In situ formed ultrafine NbTi nanocrystals from a NbTiC solid-solution MXene for hydrogen storage in MgH_2. J. Mater. Chem. A 2019;7:14244-52.

[122] Zhao-Karger Z, Hu J, Roth A, Wang D, Kuebel C, Lohstroh W, Fichtner M. Altered thermodynamic and kinetic properties of MgH_2 infiltrated in microporous scaffold. Chem. Commun. 2010;46:8353-5.

[123] Koukaras EN, Zdets AD, Sigalas MM. Ab initio study of magnesium and magnesium hydride nanoclusters and nanocrystals: examining optimal structures and compositions for efficient hydrogen storage. J. Am. Chem. Soc. 2012;134:15914-22.

[124] Buckley AC, Carter DJ, Sheppard DA, Buckley CE. Density functional theory calculations of magnesium hydride: A comparison of bulk and nanoparticle thermodynamics. J. Phys. Chem. C 2012;116:17985-90.

[125] Jia Y, Sun CH, Cheng LN, Wahab MA, Cui J, Zou J, Zhu M, Yao XD. Destabilization of Mg-H bonding through nano-interfacial confinement by unsaturated carbon for hydrogen desorption from MgH_2. Phys. Chem. Chem. Phys. 2013;15:5814-20.

[126] Vajeeston P, Sartori S, Ravindran P, Knudsen KD, Hauback B, Fjellvåg H. MgH_2 in carbon scaffolds: A combined experimental and theoretical investigation. J. Phys. Chem. C 2012;116:21139-47.

Figure Captions

Figure 1. Different hydrogen adsorption sites on Mg slab: (a) surface, (b) top tetrahedral interstices, (c) blow tetrahedral interstices and (d) octahedral interstice at the second layer [62]. Reproduced with permission from [62],copyright 2020 American Chemical Society.

Figure 2. Hydrogen adsorption sites at (a) surface and (b) inner of Mg(0001) slab, (c) Mg(0001)/TiAl(111) interface, (d) Mg(0001)/TiAl(110) interface [74]. Reproduced with permission from [74], copyright 2013 American Chemical Society.

Figure 3 (a) TEM image of AlV_3 decorated $Mg@Mg_{17}Al_{12}$ nanocomposite, (b-d) calculated absorption sites for hydrogen at AlV_3 surface and (e) dissociation barrier diagrams of hydrogen molecules on AlV_3 surfaces [62]. Reproduced with permission from [62], copyright 2020 American Chemical Society.

Figure 4. X-ray diffraction (XRD) patterns of Mg thin film deposited at (a) 1.4×10^{-2} Pa, (b) 5.6×10^{-1} Pa and (c) 1.4×10^{-1} Pa, respectively. XTEM images of the (d) Mg thin film, films with (e) Mg (0001) texture and (f) (0001)+$(10\bar{1}3)$ texture. The pathways and energy barriers of H penetration on (g) Mg$(10\bar{1}3)$ and (h) Mg(0001) surfaces [81,87]. Reproduced with permissions from [81], copyright 2019 Elsevier and [87] 2015 Nature Publishing. Migration paths (i) and corresponding energy barriers (j) for hydrogen atoms at the Mg/YH_2 interface [89]. Reproduced with permission from [89], copyright 2017 Royal Society of Chemistry.

Figure 5. (a) Schematic summary of hydrogenation mechanism of a surface-oxidized

Mg film through Pd nanoparticles, energy barriers for hydrogen diffusion perpendicular to (b) Pd(H)-Mg, (c) Pd(H)-MgO, and (d) PdH-MgH_2 interfaces [91]. Reproduced with permission from [91], copyright 2017 John Wiley and Sons.

Figure 6. (a) Front and side views of supercells of interfaces for (b) Mg($10\bar{1}0$)/MgH_2 (210), (c) Mg(0001)/MgH_2 (101) and (d) Mg($10\bar{1}0$)/MgH_2 (101) [111]. Reproduced with permission from [111], copyright 2014 AIP Publishing.

Figure 7. Theoretical calculation results for the Mg@Pt composite. Interstitial hydrogen atom (a) in the tetrahedral sites, (b) in the octahedral sites of Mg_3Pt, (c) defect formation energy of H atom dependence on hydrogen pressure at the tetrahedral and octahedral site, (d) TEM image of the Mg@Pt composite [116]. Reproduced with permission from [116], copyright 2019 Royal Society of Chemistry.

Figure 8. (a) TEM image of MgH_2/N-Nb_2O_5 composite, the initial (b) Nb-O, (c) Nb-N-O and calculated (d) Nb-O, (e) Nb-N-O clusters on the MgH_2 (110) face, (f) DOS of the MgH_2 (110) crystal face, Nb-O and Nb-N-O doped MgH_2. Color codes: white is hydrogen, orange is Mg, blue is Nb, red is O and green is N [117]. Reproduced with permission from [117], copyright 2019 Elsevier.